REPORT DOCUMENTATION PAGE

Form Approved OMB NO. 0704-0188

1. REPORT DATE (DD-MM-YYYY)	2. REPORT TYPE	3. DATES COVERED (From - To)
13-07-2010	Final Report	9-May-2007 - 8-May-2009

4. TITLE AND SUBTITLE
Enhancement of Oscillatory Flap Propulsors for Low Speed Flows in Water

5a. CONTRACT NUMBER
W911NF-07-1-0288

5b. GRANT NUMBER

5c. PROGRAM ELEMENT NUMBER
7620AI

6. AUTHORS
Laurens E. Howle

5d. PROJECT NUMBER

5e. TASK NUMBER

5f. WORK UNIT NUMBER

7. PERFORMING ORGANIZATION NAMES AND ADDRESSES
Duke University
Office of Research Support
Duke University
Durham, NC 27705 -

8. PERFORMING ORGANIZATION REPORT NUMBER

9. SPONSORING/MONITORING AGENCY NAME(S) AND ADDRESS(ES)
U.S. Army Research Office
P.O. Box 12211
Research Triangle Park, NC 27709-2211

10. SPONSOR/MONITOR'S ACRONYM(S)
ARO

11. SPONSOR/MONITOR'S REPORT NUMBER(S)
53033-MS-DRP.1

12. DISTRIBUTION AVAILIBILITY STATEMENT
Approved for Public Release; Distribution Unlimited

13. SUPPLEMENTARY NOTES
The views, opinions and/or findings contained in this report are those of the author(s) and should not contrued as an official Department of the Army position, policy or decision, unless so designated by other documentation.

14. ABSTRACT
In this report, I summarize some of my efforts in support of the DARPA Powerswim program. This report is broken down into several sections. I begin with a discussion of the kinematics of the Aquaon oscillating foil device (OFD). These kinematics are derived from digital image analysis of underwater video of combat swimmers using the OFD. Next, I derive the propulsive power requirements for divers with two gear configurations. From these results, I am able to derive OFD efficiency requirements and diver swimming duration curves. Then, I discuss

15. SUBJECT TERMS
Final report

16. SECURITY CLASSIFICATION OF:			17. LIMITATION OF ABSTRACT	15. NUMBER OF PAGES	19a. NAME OF RESPONSIBLE PERSON
a. REPORT	b. ABSTRACT	c. THIS PAGE			Laurens Howle
UU	UU	UU	UU		19b. TELEPHONE NUMBER: 919-660-5331

Report Title

Enhancement of Oscillatory Flap Propulsors for Low Speed Flows in Water

ABSTRACT

In this report, I summarize some of my efforts in support of the DARPA Powerswim program. This report is broken down into several sections. I begin with a discussion of the kinematics of the Aquaon oscillating foil device (OFD). These kinematics are derived from digital image analysis of underwater video of combat swimmers using the OFD. Next, I derive the propulsive power requirements for divers with two gear configurations. From these results, I am able to derive OFD efficiency requirements and diver swimming duration curves. Then, I discuss wing tip shapes and make suggestions for tip modifications. The next three sections discuss the role of the rear stabilizer wing and make suggestions for modifications that will allow for reduced drag and greater efficiency. This report concludes with the disclosure of an new, folding, more efficient OFD and high performance SCUBA flippers that could be a possible alternative to the OFD.

List of papers submitted or published that acknowledge ARO support during this reporting period. List the papers, including journal references, in the following categories:

(a) Papers published in peer-reviewed journals (N/A for none)

Number of Papers published in peer-reviewed journals: 0.00

(b) Papers published in non-peer-reviewed journals or in conference proceedings (N/A for none)

Number of Papers published in non peer-reviewed journals: 0.00

(c) Presentations

Number of Presentations: 0.00

Non Peer-Reviewed Conference Proceeding publications (other than abstracts):

Number of Non Peer-Reviewed Conference Proceeding publications (other than abstracts): 0

Peer-Reviewed Conference Proceeding publications (other than abstracts):

Number of Peer-Reviewed Conference Proceeding publications (other than abstracts): 0

(d) Manuscripts

Number of Manuscripts: 0.00

Patents Submitted

Patents Awarded

Awards

Graduate Students

NAME	PERCENT_SUPPORTED

FTE Equivalent:
Total Number:

Names of Post Doctorates

NAME	PERCENT_SUPPORTED

FTE Equivalent:
Total Number:

Names of Faculty Supported

NAME	PERCENT_SUPPORTED

FTE Equivalent:
Total Number:

Names of Under Graduate students supported

NAME	PERCENT_SUPPORTED

FTE Equivalent:
Total Number:

Student Metrics

This section only applies to graduating undergraduates supported by this agreement in this reporting period

The number of undergraduates funded by this agreement who graduated during this period:	0.00
The number of undergraduates funded by this agreement who graduated during this period with a degree in science, mathematics, engineering, or technology fields:.....	0.00
The number of undergraduates funded by your agreement who graduated during this period and will continue to pursue a graduate or Ph.D. degree in science, mathematics, engineering, or technology fields:.....	0.00
Number of graduating undergraduates who achieved a 3.5 GPA to 4.0 (4.0 max scale):	0.00
Number of graduating undergraduates funded by a DoD funded Center of Excellence grant for Education, Research and Engineering:	0.00
The number of undergraduates funded by your agreement who graduated during this period and intend to work for the Department of Defense	0.00
The number of undergraduates funded by your agreement who graduated during this period and will receive scholarships or fellowships for further studies in science, mathematics, engineering or technology fields:	0.00

Names of Personnel receiving masters degrees

NAME

Total Number:

Names of personnel receiving PHDs

NAME
Total Number:

Names of other research staff

NAME	PERCENT SUPPORTED
FTE Equivalent:	
Total Number:	

Sub Contractors (DD882)

Inventions (DD882)

Scientific Progress

Technology Transfer

Enhancement of Oscillatory Flap Propulsors for Low Speed Flows in Water

A Completion Report for Agreement Number W911NF-07-1-0288

AMSRD-ARL-RO-OI Proposal Number: 53033-MS-DRP.

Laurens E. Howle, Ph.D., P.E.
Associate Professor of Mechanical Engineering and Materials Science
Duke University
144 Hudson Hall
Research Drive
Durham, North Carolina 27708-0300
919.660.5331 (office)
919.660.8963 (fax)
laurens.howle@duke.edu

Executive summary

In this report, I summarize some of my efforts in support of the DARPA Powerswim program. This report is broken down into several sections. I begin with a discussion of the kinematics of the Aquaon oscillating foil device (OFD). These kinematics are derived from digital image analysis of underwater video of combat swimmers using the OFD. Next, I derive the propulsive power requirements for divers with two gear configurations. From these results, I am able to derive OFD efficiency requirements and diver swimming duration curves. Then, I discuss wing tip shapes and make suggestions for tip modifications. The next three sections discuss the role of the rear stabilizer wing and make suggestions for modifications that will allow for reduced drag and greater efficiency. This report concludes with the disclosure of an new, folding, more efficient OFD and high performance SCUBA flippers that could be a possible alternative to the OFD.

Kinematic Analysis

In order to analyze the kinematic time-history of the OFD wing motion, I used After Effects[1] to track the motion and orientation of the OFD wings. I have several digital videos of the OFD in water tunnel tests. A frame from one of the movies is shown in Figure 1. In both movies, the wing flapping frequency is $1 \pm 0.07 Hz$, the forward wing flapping amplitude is $1.4\,ft$, the surge amplitude is $0.4\,ft$ and the angular excursion of the leading wing (relative to the background – corrected for camera orientation) is $+54$ to -28 degrees. The average Reynolds number for the forward wing for a $1kt$ swimming speed is $\mathrm{Re} = 8.7x10^4$ and for a $2kt$ swimming speed is $\mathrm{Re} = 1.2x10^5$. In this Reynolds number regime, the flow over the wing should be laminar but will still be Reynolds number dependent.

Figure 1. Combat swimmer with Aquaon OFD. The forward wing provides thrust while the rear wing balances moments [1].

A time-history of the forward wing angle of attack (AoA) over one flapping cycle is shown in Figure 2. The black (red) symbols correspond to a $1kt$ ($2kt$) swimming speed. The blue lines are the likely stall limits for this chord shape and Reynolds number regime. That is, AoA below the lower blue line and

[1] After Effects is a trademark of Adobe Corporation.

above the upper blue line likely creates stalled flow. As a result, the wing produces a lower thrust and greater drag while stalled. Note that the data are noisy due to the camera location and motion relative to the swimmer. Three observations can be made by inspection of Figure 2. First, the AoA schedule is strongly dependent on swimming speed. One could either choose a target swimming speed and design

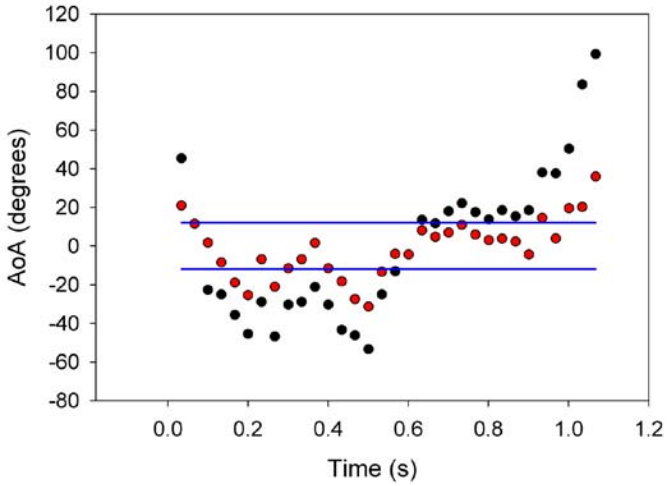

Figure 2. Time history of the forward wing angle of attack (AoA) over one period of flapping. The black and red symbols indicate the history for one knot and two knot swimming speeds, respectively. The blue line shows the likely stall limits.

the AoA history for that point or design speed-dependent AoA schedules – perhaps with nonlinear restoring springs in the wing pivot. Second, the wing spends some amount of time in the stalled configuration. This indicates that the wing produces less thrust and more drag than it should. Third, the downward stroke ($time < 0.5s$) is more stalled than the upward stroke. This information can be used to tune the pivot limits and restoring springs on the OFD.

Optimal wing actuation schedule and wing shape

In order to find a wing motion for flapping flight or undulatory swimming that produces required thrust, lift, and moments for the minimum loss, we developed a method to solve the "inverse problem" [2-3]. The methods we have previously developed for optimal flapping flight analysis are quite general and can easily be applied to PowerSwim devices. Note that this is not an extensive CFD code but uses reduced-order methods and is time-efficient. For a given lift, thrust, side-force, and moment requirement, the optimal vorticity distribution can be found in a matter of tens of minutes to, perhaps, a few hours. The inverse problem – that of finding the time history of wing motion – generally takes tens of hours to complete.

Propulsive power requirement

In this section, I consider the power required to propel a diver with mission gear through the water at a steady speed for the two cases of a diver with and without a rucksack. The required propulsive power, P, is calculated for these two cases over the range of swimming speeds $0.5kt < s < 2.5kt$. The total

diver power output, P_O, is defined in terms of the power losses from ten individual factors and is combined with the required propulsive power to define a propulsive efficiency, η. In addition, I use estimates of the endurance time limit for the two cases of a healthy adult and a peak-performance athlete to derive expressions for swimming endurance time as a function of swimming speed and efficiency of the OFD. As I show below, the best possible combination of gear and performance, a peak-performance athlete with mission gear but no rucksack, requires a minimum OFD efficiency of $\eta = 27\%$ for sustained swimming (endurance time up to eight hours) at a speed of $s = 2kt$. For the worst combination of gear and performance, a healthy adult with a ruck sack, an OFD efficiency of greater than $\eta = 45\%$ is needed for swimming at $s = 2kt$ but the endurance time is less than one hour. These results are intended to aid in selecting OFD efficiency goals given the mission requirements.

Measurements of diver drag were made by Navy personnel [4] and are duplicated in tables 1 (without ruck) and 2 (with ruck) along with the required propulsive power, P. Note that this propulsive power,

$$P = Ts \qquad (1)$$

where T is the required propulsor thrust and s is the speed, is an expression for the useful propulsive power only and does not include power losses due to inefficiencies. The inefficiencies are listed in a separate section of this report. For the case of a diver swimming at constant speed and constant depth, the required thrust is equal to the total drag on the diver. The diver drag measurements in [4] do not include drag contributions such as the induced drag created by swimming motion and drag from the OFD.

Speed, kt (fps)	Diver drag w/ gear wo/ ruck sack, lbf	Thrust power, W (hp)
0.5 (0.8)	0.19	0.22 (2.9e-4)
1.0 (1.7)	3.71	8.5 (1.1e-2)
1.5 (2.5)	9.76	34 (8.0e-2)
2.0 (3.4)	17.49	80 (0.11)
2.5 (4.2)	28.07	160 (0.22)

Table 1. Propulsive power requirement for a diver with mission gear only – no ruck sack.

Speed, kt (fps)	Diver drag w/ gear and ruck sack, lbf	Thrust power, W (hp)
0.5 (0.8)	2.06	2.4 (3.2e-3)
1.0 (1.7)	5.23	12 (1.6e-2)
1.5 (2.5)	13.75	47 (6.3e-2)
2.0 (3.4)	21.29	97 (0.13)
2.5 (4.2)	36.48	209 (0.28)

Table 2. Propulsive power requirement for a diver with mission gear and ruck sack.

In Figure 3, the required propulsive power is plotted for this same range of swimming speeds for both gear configurations. Also shown in this figure, is a cubic polynomial fitted to each of the gear configuration cases.

For the mission gear only configuration, the required propulsive power, in Watts, is fitted $\left(r^2 = 0.9999\right)$ by the cubic polynomial in swimming speed, s, in knots, by the equation

$$P = -2.2960W + \frac{3.6933W}{kt}s - \frac{3.5000W}{kt^2}s^2 + \frac{11.1876W}{kt^3}s^3 \quad . \qquad (2)$$

For the case of a diver with mission gear and rucksack, the required propulsive power is $\left(r^2 = 0.9983\right)$,

$$P = -17.3200W + \frac{55.2000W}{kt}s - \frac{47.0000W}{kt^2}s^2 + \frac{24.4000W}{kt^3}s^3 \quad . \qquad (3)$$

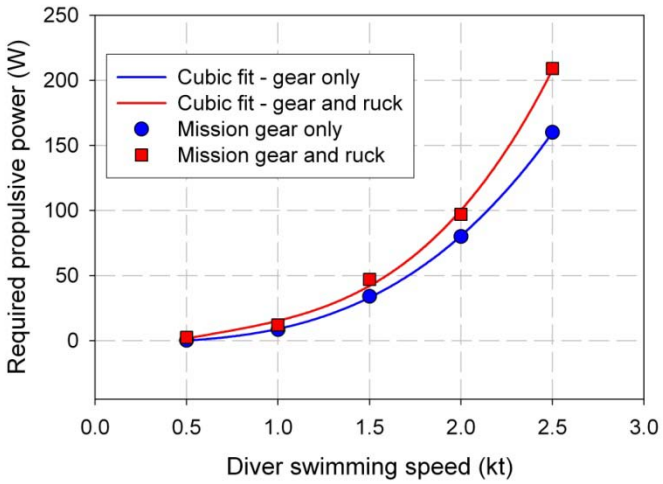

Figure 3. Ideal propulsive power requirements for a diver with mission gear only (blue circles) and for a diver with mission gear and rucksack (red squares). The solid lines represent city cubic polynomials.

Human endurance time as a function of power output

In this subsection, I list expressions for the endurance time for a healthy adult and for a peak-performance athlete. These curves of endurance time as a function of power output are available in [5] and are reproduced from (Makewicki, D. 1983)[2]. These are appropriate for cycling motion and should be used cautiously for other activities.

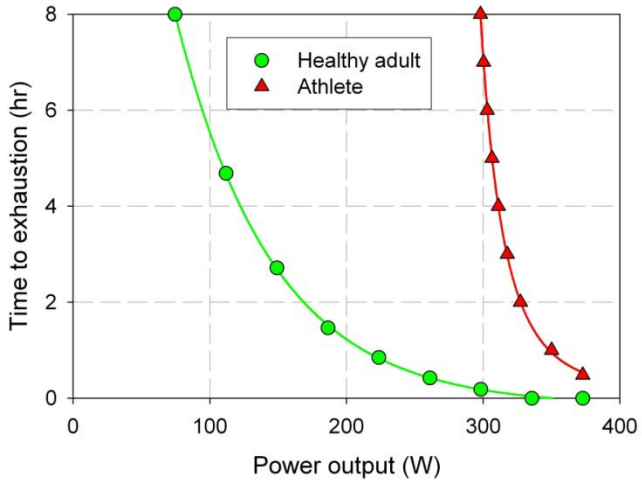

Figure 4. Endurance limit for a given power output for a healthy adult and for a peak-performance athlete.

[2] I do not have access to the original data.

The endurance time limit, t^*, of a healthy adult for exercise times $t < 8hrs$ and for total power outputs in the range $80W < P_O < 375W$ can be approximated by

$$t^* = -0.1672hrs + 23.4071hrs\left(e^{-\frac{0.0141}{W}P_O}\right) \quad (4)$$

while a peak-performance athlete with the same exercise time range and for power outputs in the range $300W < P_O < 375W$ has an approximate endurance limit of

$$t^* = 0.0071hrs\left(e^{\frac{840.22W}{P_O - 178.31W}}\right) \quad . \quad (5)$$

These functions, together with the data used in making these fits, are plotted in Figure 4. Note that these expressions should only be used for the time and power ranges listed. Additionally, equations (4) and (5) might be considered as two boundaries of endurance time for divers with differing fitness levels.

Efficiency

For the OFD, we can define the propulsive efficiency as

$$\eta = \frac{P}{P_O} \quad (6)$$

where P is the required propulsive swimming power (equations (2) and (3)) and P_O is the total output power shown in the argument of (4) and (5). The total output power P_O includes several factors that do not directly contribute to propulsion but are, nevertheless, necessary for OFD actuation. These power losses include:

1. Profile (viscous) power loss from hydrodynamic drag on the swimmer with gear (as reported in [4]).
2. Induced power loss from leg motion. This term presents itself as an additional drag on the swimmer.
3. Profile power loss from hydrodynamic drag on the OFD rear stabilizer wing.
4. Induced power loss from time-dependent motion of the OFD rear stabilizer wing.
5. Profile power loss from the OFD beam, leg cuffs, and associated hardware.
6. Induced power loss from OFD beam motion.
7. Profile power loss from the OFD forward propulsor wing.
8. Induced power loss from the OFD forward propulsor wing motion.
9. Mechanical power loss resulting from acceleration (linear and rotational) of the OFD.
10. A power “tax” due to the stress of breathing from an UBA underwater.

A key objective in the OFD analysis is to quantify and minimize these parasitic power losses. Based on these power loss terms, we can rewrite (6) as

$$\eta = \frac{P}{P + \sum_{i=1}^{10} P_i} \tag{7}$$

where the subscript corresponds to the individual loss terms defined above.

We can now construct a swimming endurance time limit as a function of efficiency and swimming speed. By substituting the required propulsive power, P, from (2) or (3) into (6) and the result into (4) or (5), we arrive at the endurance limit as a function of swimming speed and OFD efficiency. For a peak-performance athlete, the endurance time limit is

$$t^* = ae^{\frac{b}{\eta^{-1}P + c}} = ae^{\frac{b}{\eta^{-1}\left(a_0 + a_1 s + a_2 s^2 + a_3 s^3\right) + c}} \tag{8}$$

where the constants a, b and c are listed in (5) and the polynomial coefficients are listed in either (2) or (3). Note that the use of equation (8), requires the total output power to be in the range $300W < \eta^{-1}P < 375W$ as shown in Figure 4. Alternatively, one might solve for the minimum efficiency required for a given endurance limit and required swimming speed. The endurance time as a function of swimming speed for a range of efficiencies is displayed in Figure 5 for the peak-performance athlete, mission gear without rucksack configuration. An interesting result revealed in Figure 5 is that a target swimming speed of $2.0kt$ requires a minimum OFD efficiency of at least $\eta = 0.27$ for sustained swimming. A striking feature of this analysis is that a slight change in swimming speed can change the endurance time limit substantially.

For the case of a peak-performance athlete with mission gear and rucksack, the plots of endurance time vs. swimming speed are similar in behavior to the plots in Figure 5 but are shifted to lower speeds. These results are shown in Figure 6.

For a healthy adult, the endurance time limit is approximated by

$$t^* = a + be^{c\eta^{-1}P} = a + be^{c\eta^{-1}\left(a_0 + a_1 s + a_2 s^2 + a_3 s^3\right)} \tag{9}$$

with the constants a, b and c taken from equation (4). Figures 7 and 8 show the respective plots of endurance time as a function of swimming speed for the mission gear only and mission gear with rucksack configurations.

The results shown in Figures 5-8 are useful for exploring the range of OFD performance possibilities for a target swimming speed and for a given OFD efficiency. Alternatively, these results can be used to set target OFD efficiency goals given a required swimming speed and endurance time. The ill-posedness of the endurance time of a peak-performance athlete as a function of power output results in OFD swimming speed limits that are relatively insensitive to power output (within the narrow range of powers appropriate to the use of equation (5)) but are strong functions of OFD efficiency. The power loss terms in the *Efficiency* subsection of this report list the areas in which OFD efficiency might be optimized.

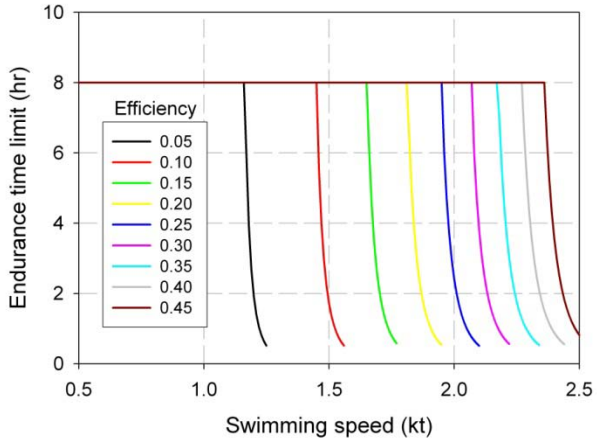

Figure 5. Endurance time limit as a function of swimming speed for a peak-performance athlete with mission gear only (no rucksack) over a range of OFD efficiencies.

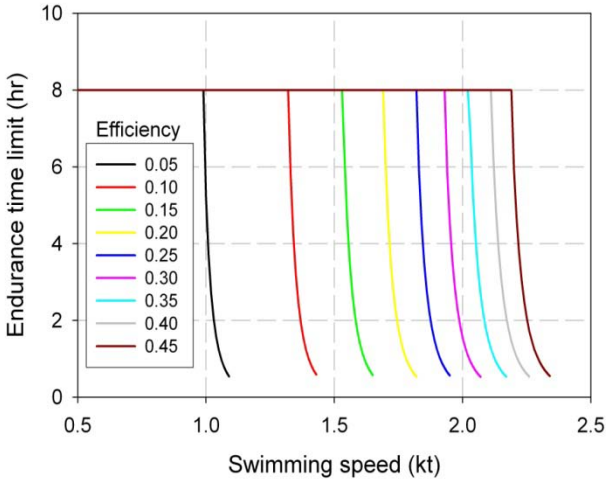

Figure 6. Endurance time limit as a function of swimming speed for a peak performance athlete with mission gear and rucksack over your range of OFD efficiencies.

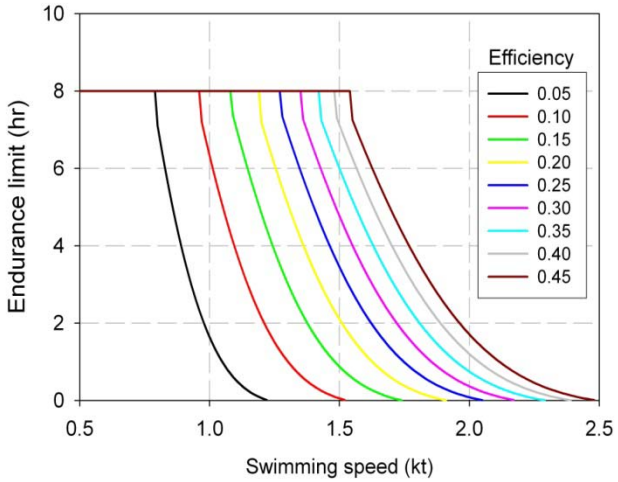

Figure 7. Endurance time limit as a function of swimming speed for a healthy adult with mission gear only no rucksack over a range of OFD efficiencies.

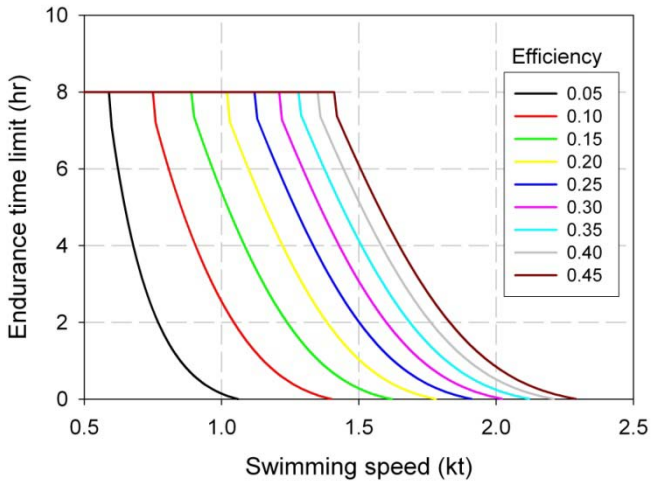

Figure 8. Endurance time limit as a function of swimming speed for a healthy athlete with mission gear and rucksack over a range of OFD efficiencies.

Wing tip shape

Recent efforts in the aeronautical community to increase the efficiency of lifting wings and thrust-producing propellers have lead to tip geometry modifications that decrease induced drag and increase efficiency. The increase in efficiency results from a reduction in the induced drag created by the lifting surface. Many of these modifications such as winglets, tip bulbs, or box wings would be inappropriate for use on the OFD due to their torque moment properties. In this report, I discuss a simple foil tip shape that will reduce the hydrodynamic drag on the forward propulsor wing of the OFD.

Modification of wing tips is aimed at decreasing the induced drag created by strong wing-tip vortices. Examples of tip modifications include end plates, sheared tips [6] as found on the Boeing 767-400, tip sails [7], tip fences such as those found on the Airbus A310, and vortex diffusers [8]. The majority of the analysis on tip devices is appropriate for Reynolds number independent flow regimes; for example, $\mathrm{Re} > 10^6$. Since the maximum Reynolds number for the OFD wing is $\mathrm{Re} < 1.5x10^5$, where Reynolds number dependence is strong, it is not clear that the tip results can be applied directly to the OFD. Additionally, the tip geometry results are strictly valid for steady flow configurations rather than the periodic flapping motion of the OFD wing. Even if the results could be applied directly to the OFD wing, the induced drag savings would likely be less than 5% [9]. As was discussed above, the power loss from the OFD forward wing induced drag is one of the many terms that account for the total power loss. Thus, winglet-type tip modifications for the OFD are expected to lead to an insignificant improvement in efficiency.

However, the increased drag from square tips is particularly pronounced for thicker airfoils. In wind tunnel tests using the NACA 0035 section at Reynolds numbers in the range $1.4x10^6 < \mathrm{Re} < 5.9x10^6$, the drag produced by square tips was found to account for *one-quarter* of the total drag on an aspect ratio 6.0 wing when compared to the same wing with rounded wing tips [10]. This result, alone, suggests that a significant drag savings would result by rounding the OFD forward wing tips.

Suggestion for an interim tip geometry

While the wing geometry of the OFD might evolve as the PowerSwim project progresses, a simple modification to the present design of the propulsor (forward) wing could reduce the induced drag created as a result of time-dependent wing motion and three-dimensional shed wake effects. This drag decreases the propulsive efficiency of the OFD and contributes to the overall power loss through term P_7 (induced power loss from the OFD forward propulsor wing) from equation (7). One possible alternative is shown in Figure 9.

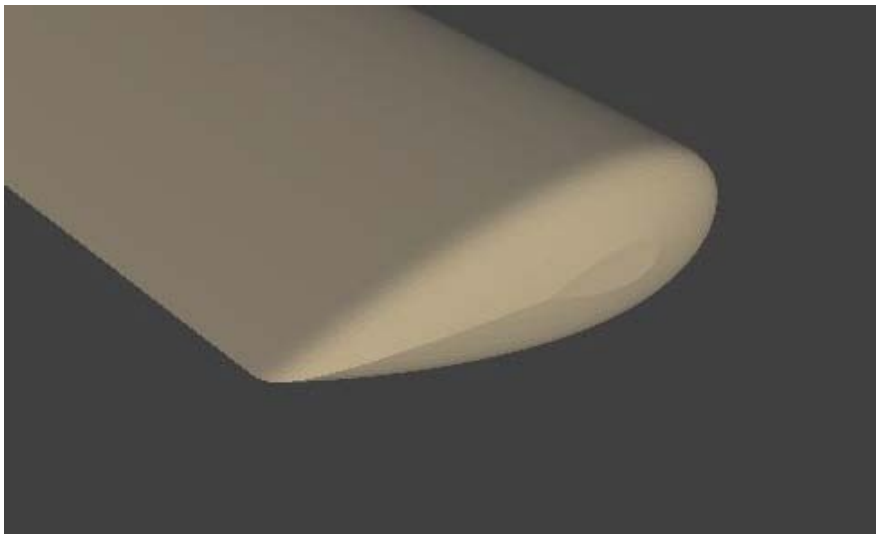

Figure 9. Tip geometry scaled according to equation (14).

This tip geometry, for a wing of span S, is scaled according to a simple transformation. Let the x coordinate correspond to the chord-wise direction (positive up-stream), the y direction orient positive upward and the z direction represent the span-wise coordinate with the origin at the wing center and increasing toward the wing tip. Let $\mathbf{p} = \left(p_x, p_y, p_z, 1 \right)^T$ denote a point on the wing surface. Likewise, let $\mathbf{p}'$ denote a transformed surface point. Then the tip geometry transforms according to

$$\mathbf{p}' = \mathbf{T}'\left(\mathbf{S}\left(\mathbf{T}\mathbf{p}\right)\right) \tag{10}$$

where $\mathbf{T}$ translates the point of maximal chordal thickness ($x/C = 0.3$ for the NACA 00XX series sections) to the $x = 0$ coordinate according to

$$\mathbf{T} = \begin{bmatrix} 1 & 0 & 0 & t_x \\ 0 & 1 & 0 & 0 \\ 0 & 0 & 1 & 0 \\ 0 & 0 & 0 & 1 \end{bmatrix} \tag{11}$$

and

$$\mathbf{T}' = \begin{bmatrix} 1 & 0 & 0 & -t_x \\ 0 & 1 & 0 & 0 \\ 0 & 0 & 1 & 0 \\ 0 & 0 & 0 & 1 \end{bmatrix} . \qquad (12)$$

The scaling $\mathbf{S}$ is defined by

$$\mathbf{S} = \begin{bmatrix} f\left(\frac{z}{S}\right) & 0 & 0 & 0 \\ 0 & f\left(\frac{z}{S}\right) & 0 & 0 \\ 0 & 0 & 1 & 0 \\ 0 & 0 & 0 & 1 \end{bmatrix} \qquad (13)$$

with

$$f\left(\frac{z}{S}\right) = \begin{cases} 1 & \forall \ \frac{z}{S} < \frac{31}{2^5} \\ 1 - 3 \bullet 2^{18}\left(\frac{z}{S} - \frac{31}{2^5}\right)^4 & \forall \ \frac{31}{2^5} \le \frac{z}{S} \le 1 \end{cases} . \qquad (14)$$

This tip scaling has been used successfully in our wind tunnel studies of humpback whale flippers [11] for Reynolds numbers similar to those of the OFD.

Another alternative would be to create a surface of revolution at the tip. This surface would revolve about the chord line and would be similar to the tip shape found on the OFD rear stabilizer wing. This approach will be particularly easy to accomplish due to the symmetric wing section (NACA 0035) presently used on the OFD forward wing.

Wing tip geometry modifications aimed at reducing the induced drag on lifting surfaces has received considerable recent attention [12]. Many of the tip shapes considered in the literature would be inappropriate for use on the OFD forward wing due to the need for control over the wing's moment characteristics. At present, a simple rounded tip should be advantageous in reducing the induced drag on the forward OFD wing while requiring a modest modification to the present geometry.

Rear wing kinematics

The rear stabilizer wing for the OFD was analyzed for lift, drag, and power requirement. Digitized video images from the 2006 Carderock tests were used to measure the motion of actuation over one cycle of swimming movement. I used Mark Drela's XFoil program to estimate lift drag and polar data for a mean Reynolds number of $\mathrm{Re} = 65,000$ using a wing section with a blunt trailing edge and for a wing with a sharp trailing edge. These results show that a modest power savings can be gained by changing the rear stabilizer wing to a NACA 2412 section with the present planform. *An interesting result from this*

analysis is that the rear wing can be tuned to produce a portion of the total thrust required of the OFD, perhaps up to 25%.

Frames 17:17:06 through 17:18:06 from the video *PowerSwim Clip 05.mpg* were digitized. I extracted pixel coordinates for the leading and trailing edges of both the stabilizer wing and the propulsor flap as well as several reference locations. The reference locations were needed to scale the pixel coordinates into physical coordinates and to correct the image for camera tilt and movement relative to the swimmer. The coordinates of the leading and trailing edges of the rear flap were then used to generate the time history of motion over one cycle of OFD actuation. Digitizing the movie frames creates an inherently noisy time sequence. In order to filter the noise, I used a four-mode Fourier series as in my previous kinematic analysis. A plot of the horizontal and vertical positions of the trailing edge of the rear stabilizing wing over one cycle of OFD actuation is shown in Figure 10. The coordinate system origin is arbitrary. As an alternate view, the limit cycle is shown in Figure 11. This figure demonstrates the complicated motion generated by OFD actuation.

In this sequence of images, the swimming speed is known to be 1.5 knots. With the combination of the known swimming speed and the measured flap motion, we can derive the local angle of attack between the rear stabilizer flap and the oncoming flow. In Figure 12, I show the geometric wing angle and the angle of attack over one cycle of actuation. The geometric wing angle is measured directly from the images. Note that the local angle of attack, which includes the geometric angle and the motion-induced relative velocity, is probably stalled over a portion of the actuation cycle. However, it is not possible to know from these images whether or not stall occurs, as stall takes some time to initiate. In other words the dynamic motion of the wing might prevent stall from occurring. One can visually test for stall by using streamers as we did in the Key West tests. The streamers should be placed near the trailing edge.

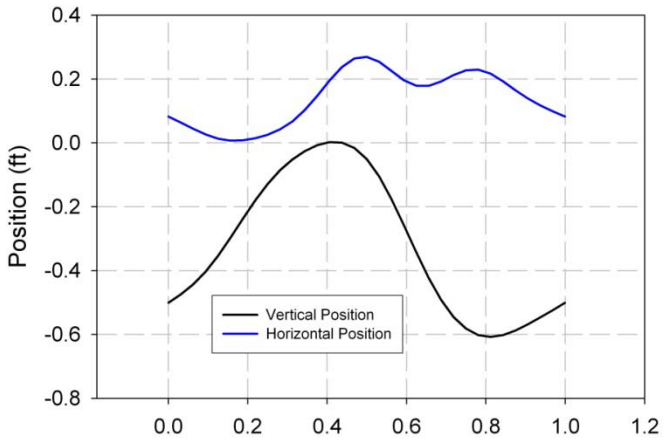

Figure 10. Time history of the rear stabilizer wing training edge. The coordinate system origin is arbitrary.

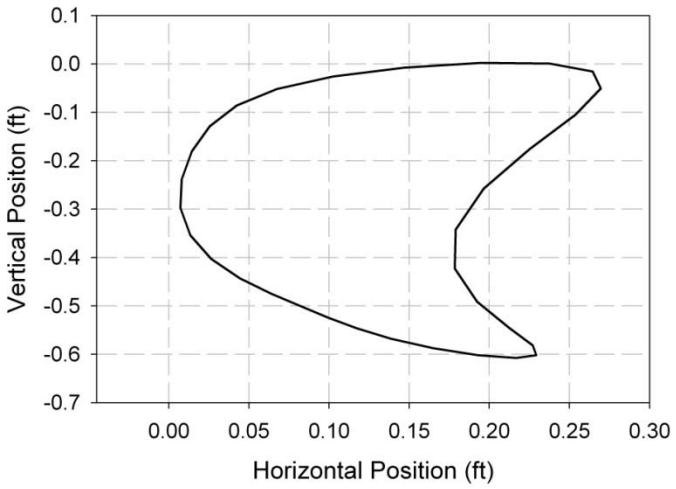

Figure 11. Rear wing trailing edge limit cycle (arbitrary coordinate system origin).

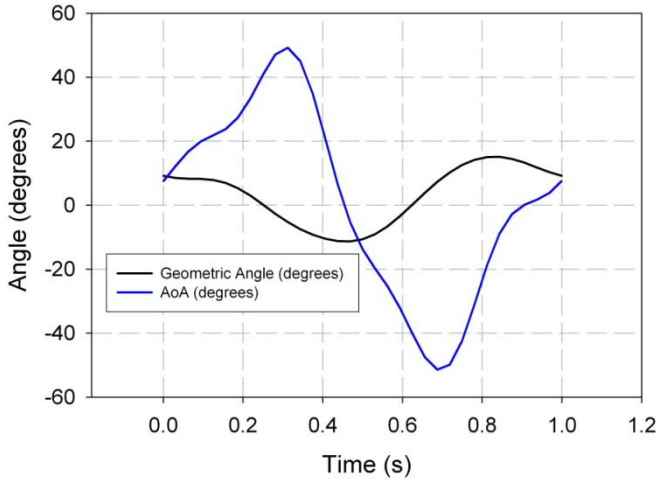

Figure 12. Rear stabilizer wing geometric angle (black) and angle of attack (blue) over one period of actuation.

Wing section geometry

The original wing geometry consists of a 20% thick section with a flat lower surface and a prominently rounded trailing edge. The wing is skinned with a fiber mesh and left unfinished. I was unable to use standard computational methods (XFoil) to analyze the present sectional performance due to the rounded trailing edge. The trailing edge caused to code to diverge and no solution was found. However, we might expect that the rounded trailing edge accelerates stall. This is due to the fact that a highly separated flow region will exist just beyond the trailing edge. A separated flow region will move past the trailing edge and along the suction surface, especially if the trailing edge is rounded.

For the purposes of comparison, I analyzed the performance of a standard NACA 2412 airfoil section for the same conditions. Two configurations were analyzed. The first configuration consisted of the standard wing section while the second configuration had a truncated, blunt trailing edge rather than the current rounded geometry. The XFoil software system was able to analyze the blunt profile without difficulty. In both cases, I used amplification factors of $n=1.0$ and $n=9.0$ in order to study the performance of both sections under turbulent and laminar conditions (respectively). I believe that the turbulent amplification factor, $n=1.0$, is more appropriate to the OFD operational conditions because the present wing geometry uses a rough skin and because the oncoming flow, as experienced by the rear stabilizer wing, is likely already turbulent due to vortex shedding from the forward propulsor wing and from the turbulent wake shed behind the Draeger UBA. The four lift-drag polars are shown in Figure 13. As is evident from the figure, the best choice for the OFD is a wing with a sharp trailing edge experiencing turbulent flow. Since the rear wing experiences turbulent flow due to upstream conditions, the rough composite skin might not be necessary to trigger turbulent flow. There might be a modest drag savings realized by producing rear stabilizer wing with smooth composite skins.

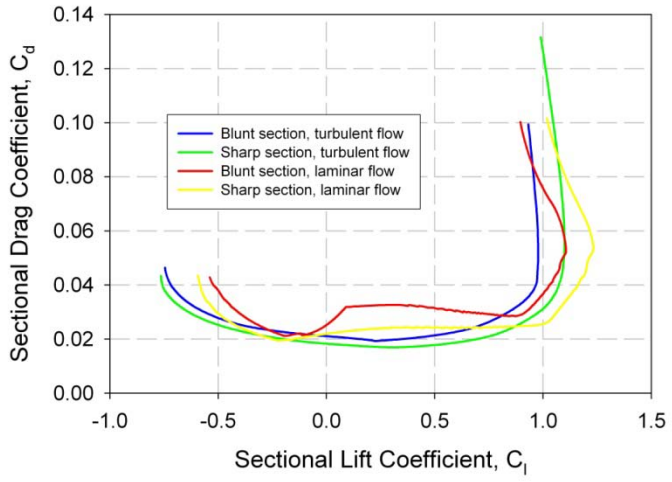

Figure 13. Lift-drag polar plots for the rear stabilizer wing using the NACA 2412 section with blunt and sharp trailing edges for laminar and turbulent flow conditions at a mean Reynolds number of 65,000.

Lift requirements

Using the measured kinematics, and the lift-drag polar for a NACA 2412 wing section, I ran my optimizer to find an estimated time averaged lift produced by the rear stabilizer wing of $F_L=-1.2lbf$. Note that the forces from the present wing are likely substantially different due to the rounded trailing edge. It is also evident from the analysis, that the rear stabilizer wing can be trimmed to produce some amount of thrust, perhaps up to 25% of the thrust required on the forward wing. A NACA 2412 foil section with the same wing dimensions undergoing the same motion as in the digitized images will have the following force and power production:

Speed	2.54 ft/s
Thrust Force	3.20 lbf
Lift Force	-1.22 lbf
Inviscid Induced Power	2.05 lbf ft/s
Viscous Profile Power	0.96 lbf ft/s
Total Power Loss	3.01 lbf ft/s
Thrust Power	8.12 lbf ft/s

If we require the wing to produce this lift and thrust, and find the minimal power loss, the total power loss drops only to 2.91 lbf ft/s. With only twist and chord as degrees of freedom, I was unable to find a wing configuration with less than 3.0 lbf ft/s. Thus, by changing the wing section to a NACA 2412 shape, a near-optimal configuration can be obtained.

The present rounded trailing edge on the rear stabilizer wing produces a configuration that stalls even at a zero-degree angle of attack. This results in a high-drag situation. Without a time-consuming CFD analysis, the lift and drag characteristics of the present section shape cannot be known. However, the rounded wing will perform worse than a wing with a blunt trailing edge. By changing the rear wing to a NACA 2412 section, a near-optimal wing configuration will be realized.

Folding, reduced-mass OFD design

One of the design requirements that had not yet been fulfilled when I was last involved with the Powerswim program, is the requirement that the OFD be foldable. In order to investigate this design requirement, I developed an independent OFD design that allows the device to be folded for storage or for transport through submarine hatches. Additionally, I wanted to be able to reduce the mass of the OFD in order to increase the mechanical efficiency associated with actuating the device. Because there is a requirement that the OFD be neutrally buoyant or slightly negatively buoyant, reducing mass also means that the volume of the OFD must be reduced. The third objective that I wanted to investigate in my redesign of the OFD is a reduction in the mass moment of inertia. This reduction in the mass moment of inertia reduces the mechanical actuation portion of the total power requirement.

In Figure 14, I show my redesigned OFD in the deployed configuration and in Figure 15, the OFD is shown in the folded configuration. Top and rear views are shown, respectively, in Figures 17 and 17. Note, in particular, the extremely streamlined design shown in the OFD rear view (Figure 17).

In order to reduce the total mass and total volume displaced by the redesigned OFD, my new design uses carbon fiber as the main structural element with foam core in the wings. The deck, calf clamps, and fuselage are all vacuum-bagged carbon fiber. Any weight that would need to be added in order to make the OFD neutral or negatively buoyant would be added as closely as possible to the center of actuation in order to reduce the mass moment of inertia. An unfinished carbon fiber deck is shown in Figure 18.

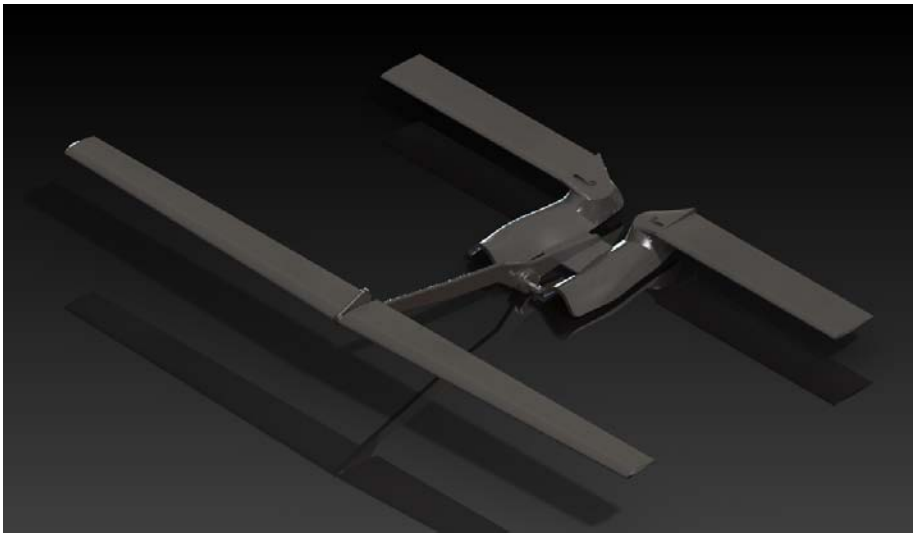

Figure 14. OFD in deployed configuration. The lower side is facing up.

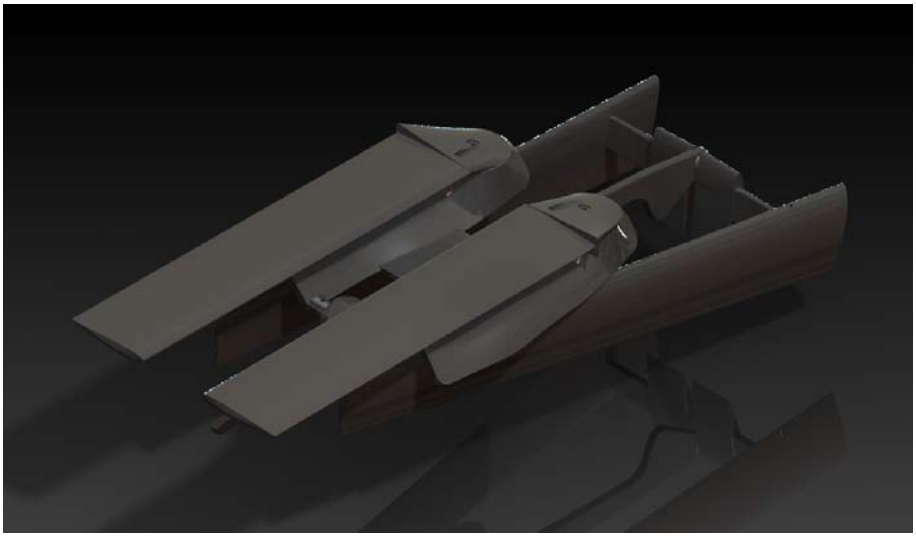

Figure 15. OFD shown in folded configuration.

Figure 16. OFD top view. The calf clamps are not shown in this image.

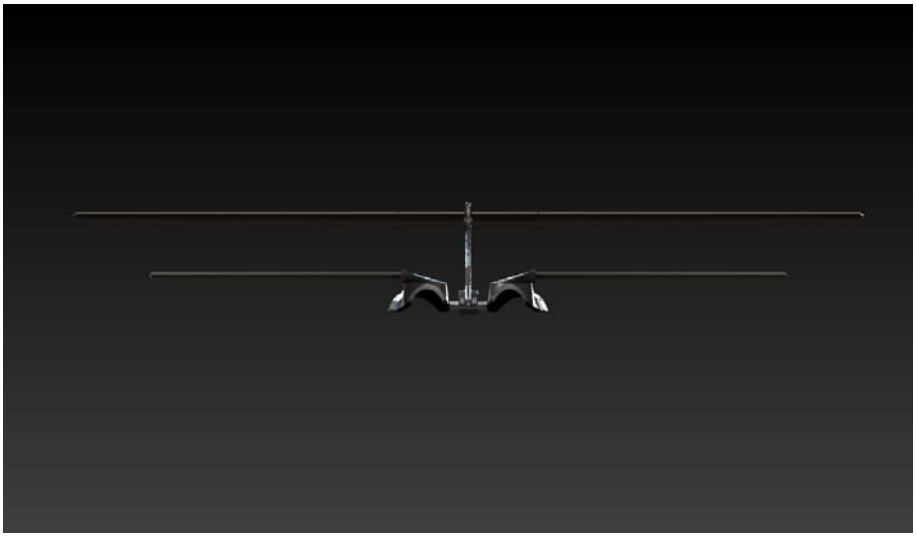

Figure 17. OFD rear view. Note low-drag configuration.

Figure 18. Vacuum bag model and unfinished carbon fiber OFD deck unit.

High efficiency flipper alternative

The possibility still exists that special warfare operators will find the OFD cumbersome, particularly when maneuvering at a mission objective site. In order to offset this potential challenge, I designed a new set of scuba flippers that are actuated by can conventional flipper kick motion. This new SCUBA flipper makes use of the plurality of high-performance foil sections that do not deform. The foil sections, as shown in Figures 19 and 20, pivot about a point close to their leading-edge. During the upstroke and downstroke, the foil sections assume an angle of attack that is advantageous to efficient thrust development. Should the DoD be interested in pursuing this flipper design, I would welcome discussing this opportunity.

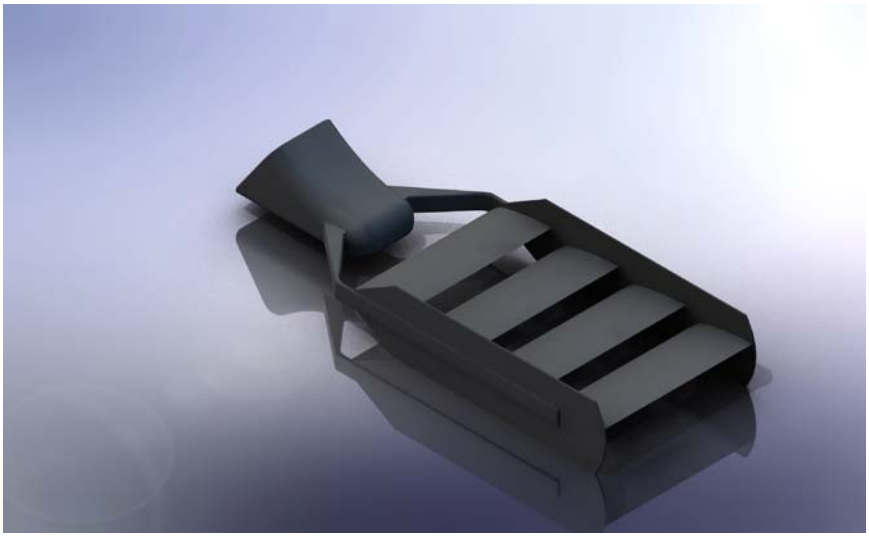

Figure 19. Venetian flipper design concept. These fins are used like standard scuba flippers. The four articulating foils have modern airfoil cross sectional shapes that allow for improved thrust and reduce drag when compared to conventional scuba flippers. The fixed side plates prevent tip loss.

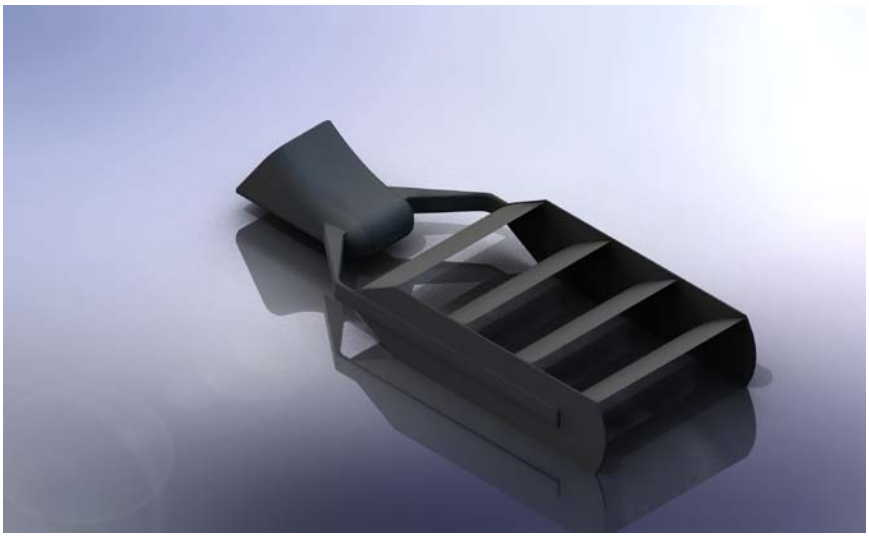

Figure 20. Foils shown in the backward kick configuration.

References

1. Stepp, D., *Image of Aquaon Oscillating Foil Device, developed by Deka Research, LLC*. 2006.
2. Hall, K.C. and L.E. Howle, *The mechanics of flapping flight.* 2005.
3. Howle, L.E. and K.C. Hall, *Optimal wing shape in flapping flight.* 2006.
4. NSWCCD, *Diver drag letter report 072606*. 2006, Carderock Division Naval Surface Warfare Center: Bethesda, MD.
5. Urieli, I. *Human Power Vehicles*. 2006 05/20/2006]; Available from: http://www.ent.ohiou.edu/~et181/hpv/hpv.html.

6. Smith, S.C. and I. Kroo, *Computation of induced drag for elliptical and cresent-shaped wings.* AIAA J. Aircr., 1993. **30**: p. 446-452.
7. Spillman, J.J., *The use of wing tip sails to reduce vortex drag.* Aeronaut. J., 1978. **82**: p. 387-395.
8. Hickett, J.E. *Vortex drag reduction by aft-mounted diffusing vanes. ICAS Pap. 80-13.4.* in *12th Conf. Int. Counc. Aeronaut. Sci.* 1980. Munich, Ger.
9. Smith, S.C., *A computational and experimental study of nonlinear aspects of induced drag. NASA TP 3598.* 1996, Natl. Aeronaut. Space Admin.: TP 3598.
10. Bullivant, W.K., *Tests of the NACA 0025 and 0035 airfoils in the full-scale wind tunnel. Report 708.* 1941, NACA.
11. Miklosovic, D.S., et al., *Leading-edge tubercles delay stall on humpback whale (Megaptera novaeangliae) flippers.* Physics of Fluids, 2004. **16**(5): p. L39-L41.
12. Kroo, I., *Drag due to lift: concepts for prediction and reduction.* Annu. Rev. Fluid Mech., 2001. **33**: p. 587-617.